Organic Matter in the Ocean

Rene M. Boiteau

Department of Chemistry, University of Minnesota, Minneapolis, Minnesota 55077, United States

College of Earth, Ocean, and Atmospheric Sciences, Oregon State University, Corvallis, Oregon 97330, United States

Erin L. McParland

Department of Marine Chemistry and Geochemistry, Woods Hole Oceanographic Institution, Woods Hole, Massachusetts 02543, United States

Figures:

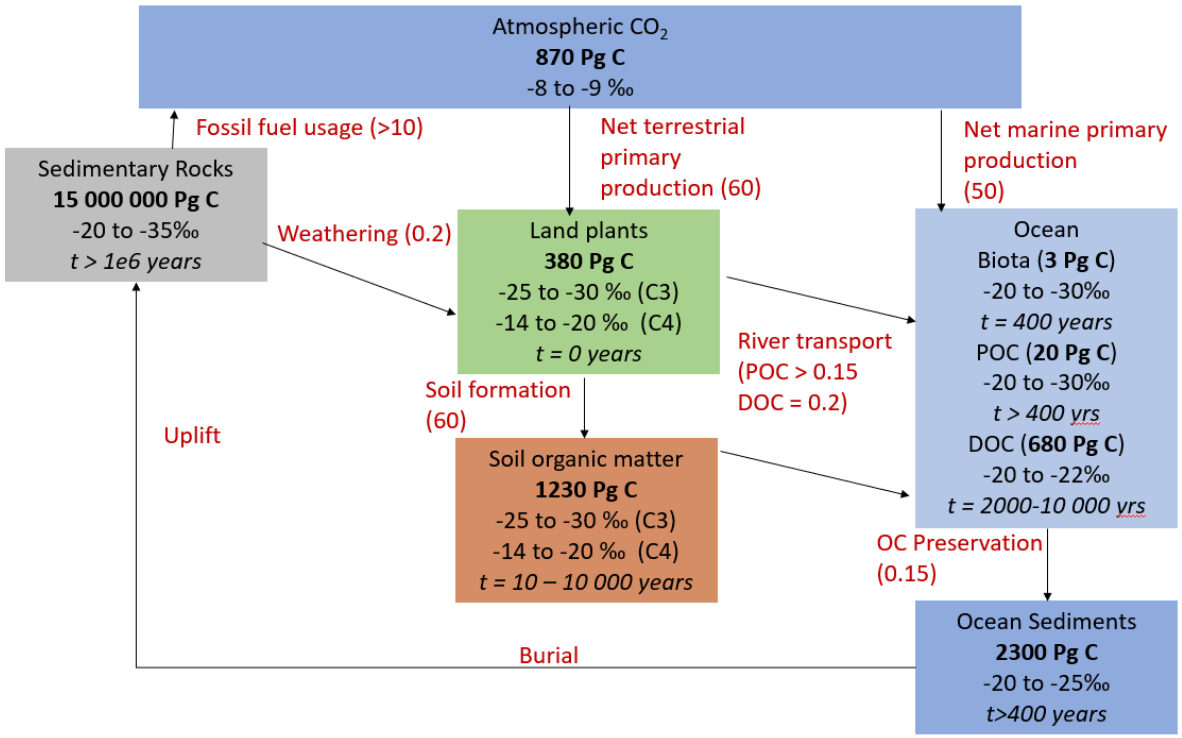

Figure 1: Global organic carbon cycle. The bold values are approximate reservoir sizes (10^{15} g C = 1 Pg) and red values are approximate fluxes (Pg C yr^{-1}). Non-bold numbers are approximate ranges for stable carbon isotopic composition ($\delta^{13}C$, per mil) and italicized numbers are approximate radiocarbon ages (yr before present). Based on Eglinton and Repeta 2014.

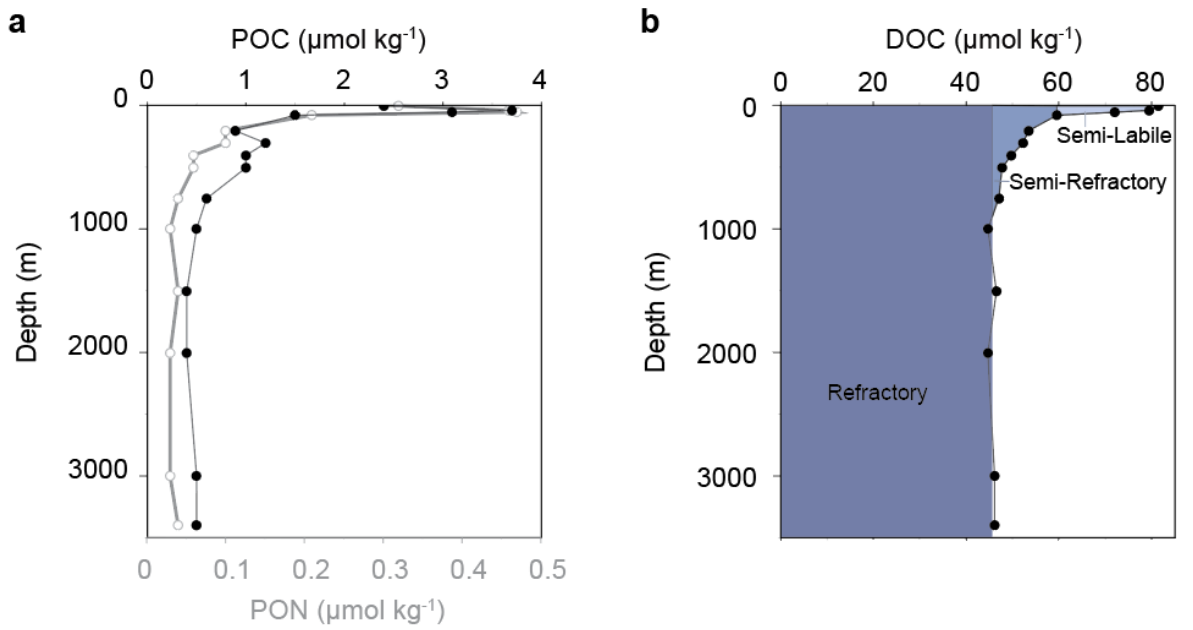

Figure 2: (a) Example depth profile of water column particulate organic carbon (POC) and particulate organic nitrogen (PON). Note the relative decrease in PON versus DOC with depth. (b) Example depth profile of dissolved organic carbon (DOC) showing observed fractions of refractory, semi-refractory (accumulating above the permanent pycnocline), and semi-labile DOM (accumulating above the seasonal pycnocline) Data from the North Atlantic Ocean; Hansell *et al.* 2021; (FLUXES I cruise; 21.5°W, 17.5°N; August, 2017).

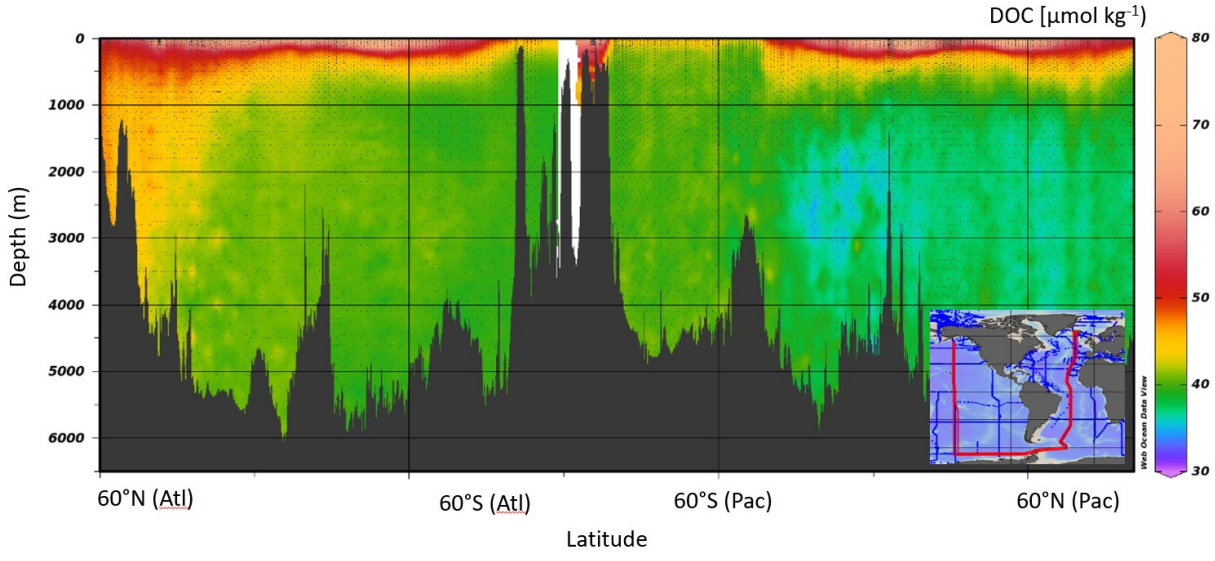

Figure 3: Section plot of dissolved organic carbon (DOC) concentrations across the Atlantic and Pacific Ocean basins. Inset map shows the defined section from the North Atlantic (starting at 20°W) across the Southern Ocean to the North Pacific (ending at 150°W). DOC concentrations are highest in the surface and then decrease gradually along the flow path of deep water overturning circulation. Data from Hansell *et al.* 2021.

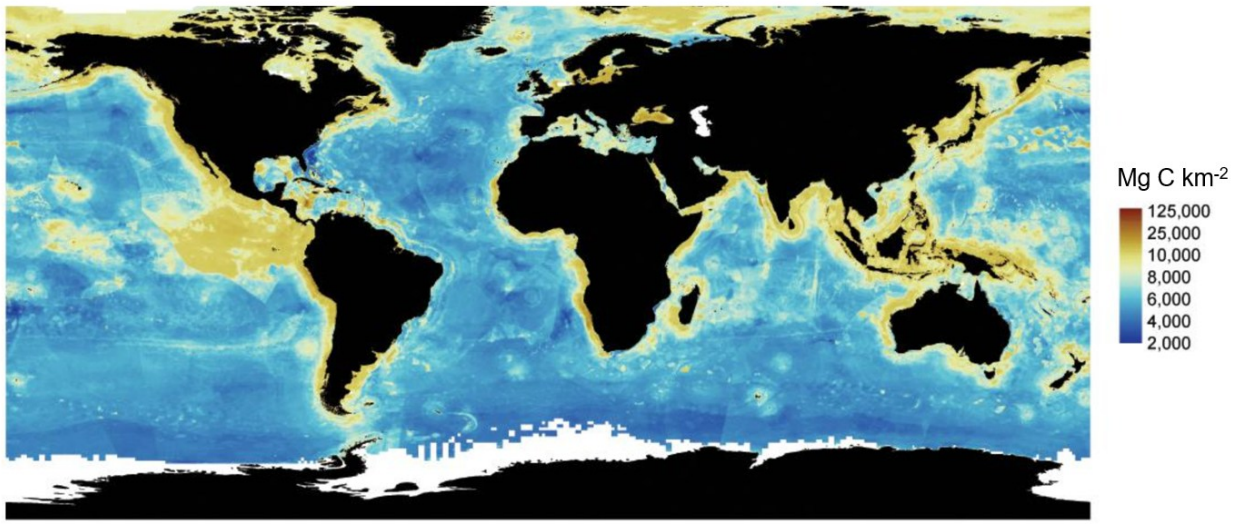

Figure 4: Average distribution of global marine sediment organic carbon stored in the top 1 m of sediment. From Atwood *et al.* 2020.

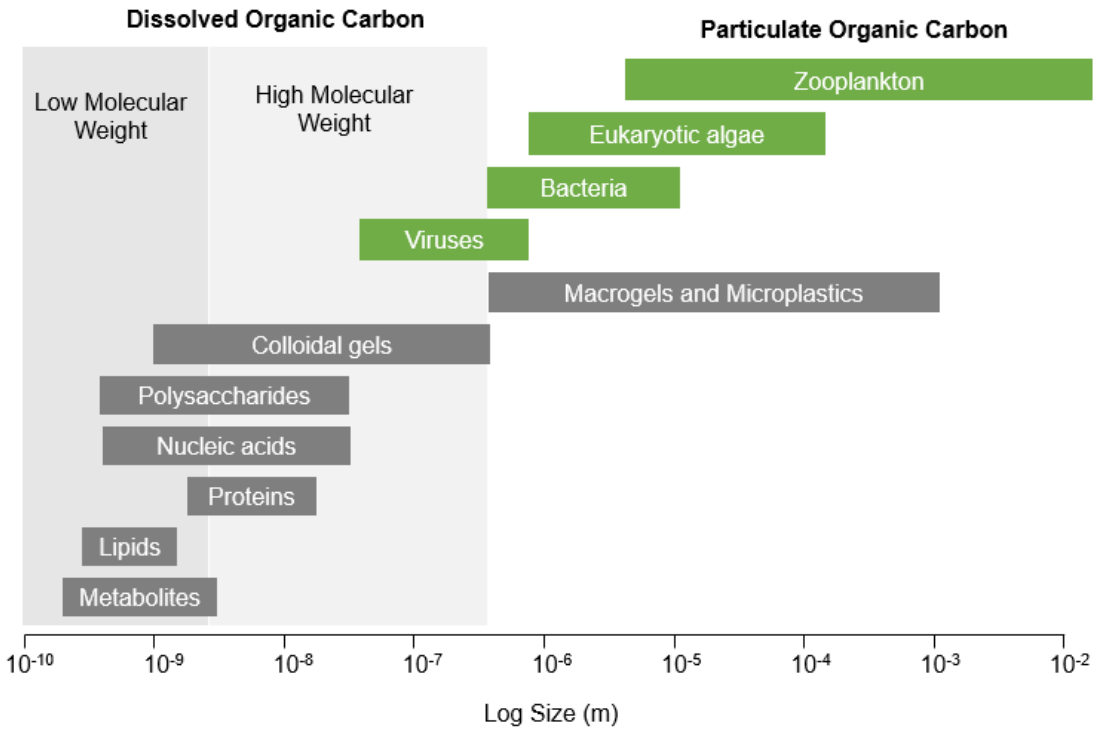

Figure 5: Size range of organic matter components present in seawater. Gray boxes correspond to molecular classes. Green boxes correspond to biological classes. Black text corresponds to operationally defined classes. Based on Verdugo *et al.* 2004.

Table 1: Approximate elemental composition of biochemical classes (Data from Geider and La Roche, 2002), and the percentage of cell mass associated with different biochemical fractions of actively growing microalgae (Data from Finkel et al. 2016)

Component	Elemental Composition	% Cell mass
Amino acids and Protein	$C_{4.43}H_7O_{1.44}N_{1.16}S_{0.019}$	30 - 34
Lipids	$C_{40}H_{74}O_5$	16-18
Carbohydrates	$C_6H_{12}O_6$	13-17
Phosphoglycerides	$C_{37.9}H_{72.5}O_{9.4}N_{0.43}P$	5-15*
RNA	$C_{9.5}H_{13.75}O_8N_{3.75}P$	4-7
Chlorophyll a	$C_{55}H_{72}O_5N_4Mg$	0.7-2
DNA	$C_{9.75}H_{14.25}O_8N_{3.75}P$	0.2-2

* Range reported by Geider and La Roche, 2002

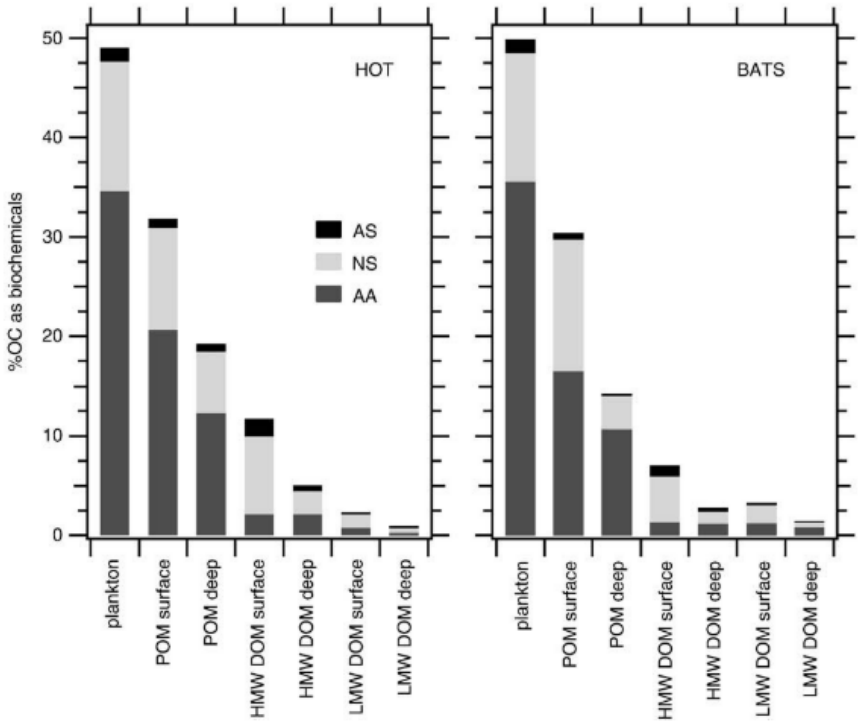

Figure 6: Carbon-normalized yields (%OC) of amino acids (AA), neutral sugars (NS) and amino sugars (AS) in plankton, suspended particulate organic matter (POM), high molecular weight dissolved organic matter (HMW DOM), and low molecular weight dissolved organic matter (DOM) from the North Pacific (HOT) and Sargasso Sea (BATS). From Kaiser and Benner, 2009.

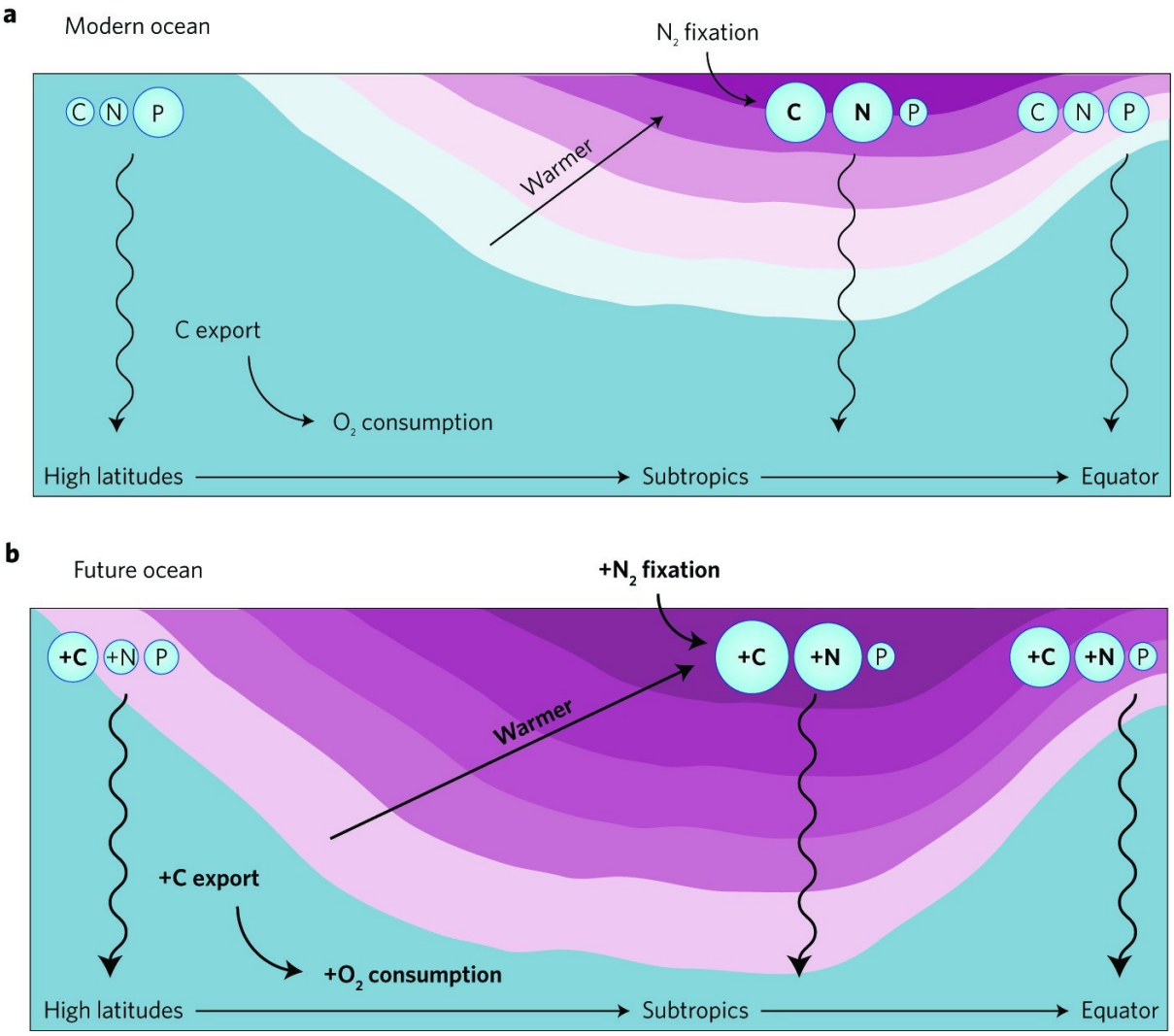

Figure 7: Variable POM stoichiometry in a changing ocean (as depicted by the colored contours which reflect an expansion of stratification and increased temperatures). In modern oceans (a), the highest C:N:P are found in the nutrient-poor, warm subtropical oceans and the lowest C:N:P are found in the nutrient replete, higher latitudes. In future oceans (b), the expansion of nutrient-poor regions will favor a higher C:N:P ratio of POM. From Devries 2018.

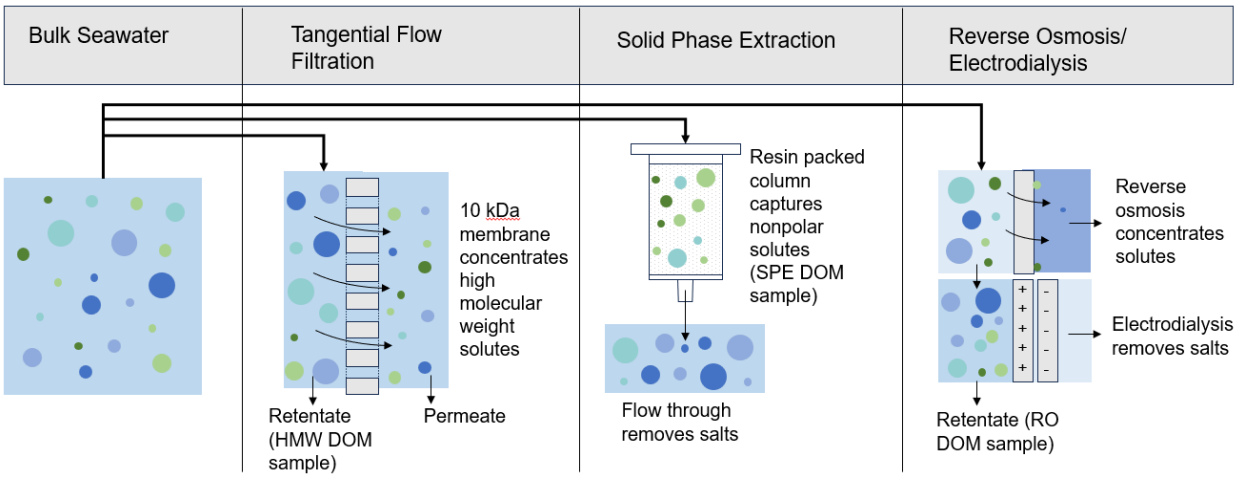

Figure 8: Strategies for recovering dissolved organic matter (DOM) from seawater. Tangential flow filtration selectively concentrates high molecular weight molecules, while solid phase extraction (SPE) selectively extracts nonpolar molecules. Reverse osmosis (RO) coupled with electrodialysis recovers the largest fraction of DOM of any single method.

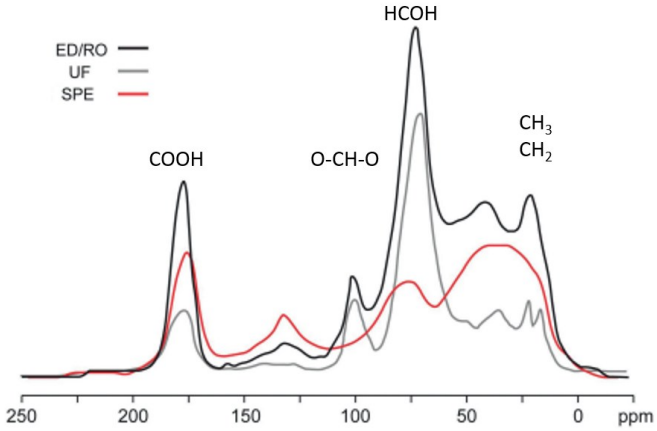

Figure 9: ^{13}C NMR of dissolved organic matter (DOM) recovered by electrodialysis/reverse osmosis (ED/RO black line) superimposed on spectra of high molecular weight DOM collected by ultrafiltration (UF, gray trace), and solid phase extracted DOM (SPE, red trace) from surface seawater. The spectra are scaled to the reverse osmosis peak at 70 ppm. Modified from Koprivnajak et al. 2009.

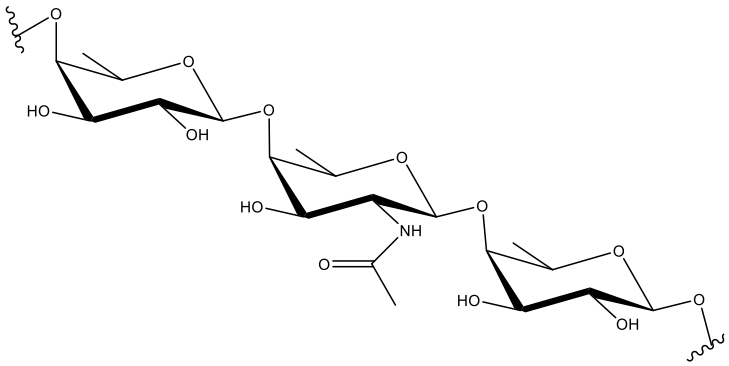

Figure 10: Example structure of high molecular weight DOM containing neutral sugars and N-acetylated sugars

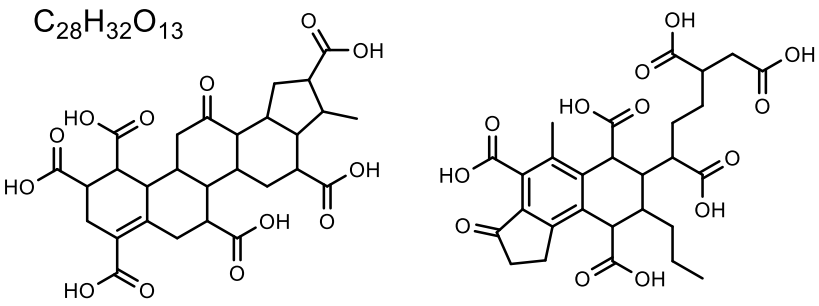

Figure 11: Structural isomers of $C_{28}H_{32}O_{13}$ that conform to the NMR patterns of carboxyl-rich alicyclic molecules (CRAM) observed in marine DOM. Based on Hertkorn et al. 2006.

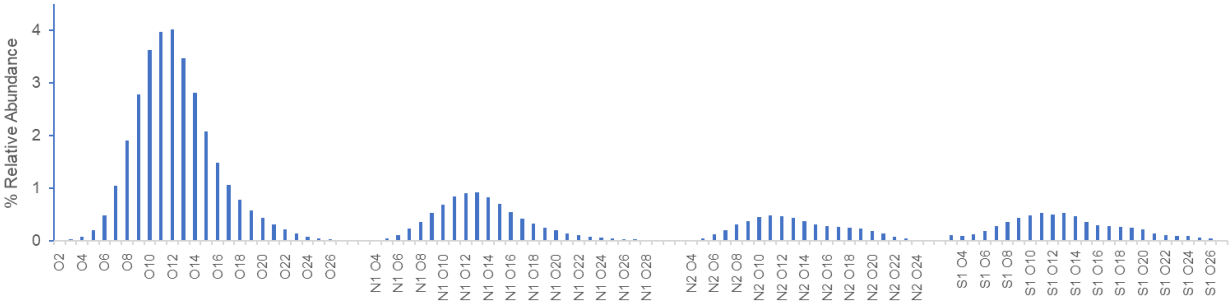

Figure 12: Class graphs comparing the number of identified peaks from FT-ICR MS analysis of DOM extracted from surface seawater by solid phase extraction. Classes group assigned peaks corresponding to formulas containing a specified number of oxygen and nitrogen atoms. Relative abundance corresponds to the sum intensity of all peaks within a class compared to the sum intensity of all assigned peaks in the spectrum. Data courtesy of Angela Knapp and Amy McKenna.

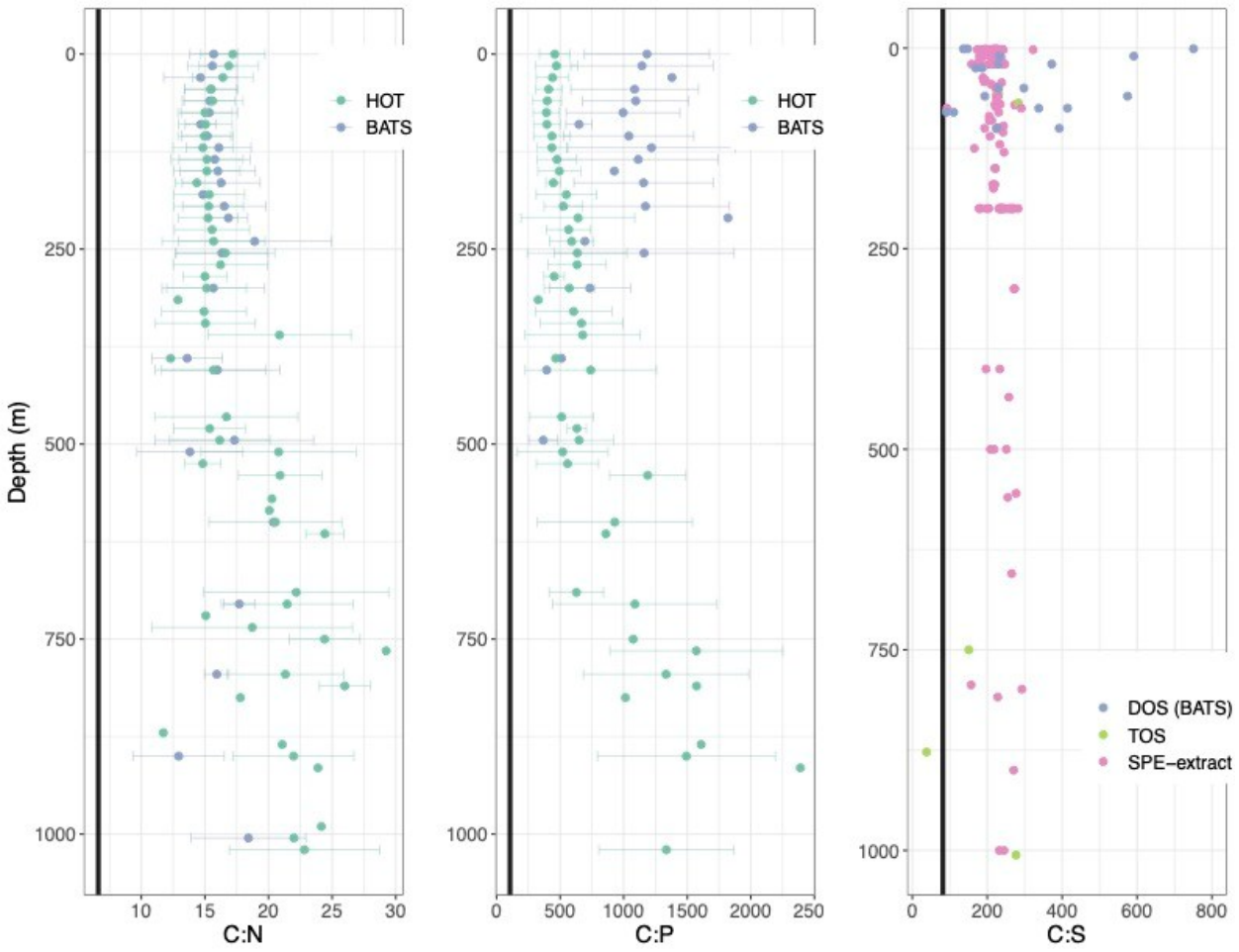

Figure 13: The stoichiometry of bulk dissolved organic matter ratios. (A) Ratios of organic carbon to nitrogen (C:N) at the Hawaiian Ocean Time-series (HOT) (green) and the Bermuda Atlantic Time-series Station (BATS) (purple). (B) Ratios of organic carbon to phosphorus (C:P) at the HOT and the BATS. Points in (A) and (B) reflect the average and error bars the standard deviation binned by 15m increments for any data available from 1988 - 2008 at HOT and 1988 - 2021 at BATS. (C) Ratios of all previous organic carbon to sulfur (C:S) ratios collected at latitudes below 32°. Dissolved organic sulfur (DOS) was measured at BATS, and here are normalized to TOC from corresponding month and year with data from the BATS program (purple). In August 1999, low DOS values of 36nM at 1m and 24nM at 100m resulted in C:S ratios of 1848 and 2693 which are cut-off from the presented data. Total organic sulfur (TOS) was measured along a transect through the Northern and Southern Atlantic Oceans, and here are normalized to corresponding reported TOC values (light green). Ratios of C:S were reported for SPE-extracted DOM collected in both the Pacific and Atlantic Oceans (pink). Black lines reflect Redfield ratios of 6.6, 106, and 81.5 for C:N, C:P, and C:S, respectively. Data from the HOT project, the BATS program, Cutter et al. (2004), Longnecker et al. (2020), Ksionzek et al. (2016), and Phillips et al. (2022).

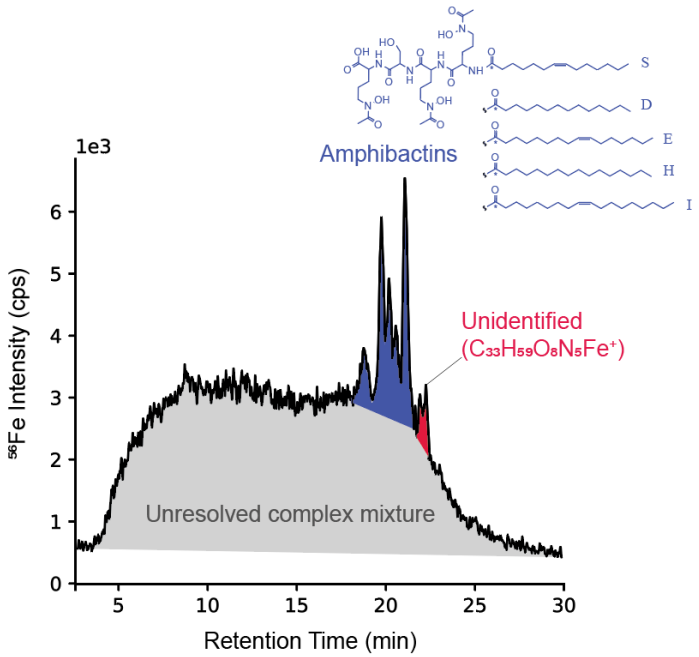

Figure 14: High pressure liquid chromatography inductively coupled plasma mass spectrometry chromatogram showing the separation and detection of organic ligands from an SPE extract of seawater collected from the Fe-limited high nitrate low chlorophyll regions of the California Current System. The colors indicate distinct co-occurring ligands including identified microbial siderophores (amphibactins, blue) and an unidentified orphan Fe-organic complex (red) superimposed on an unresolved complex mixture of polydisperse ligands (gray). Data from Boiteau *et al.* 2019.

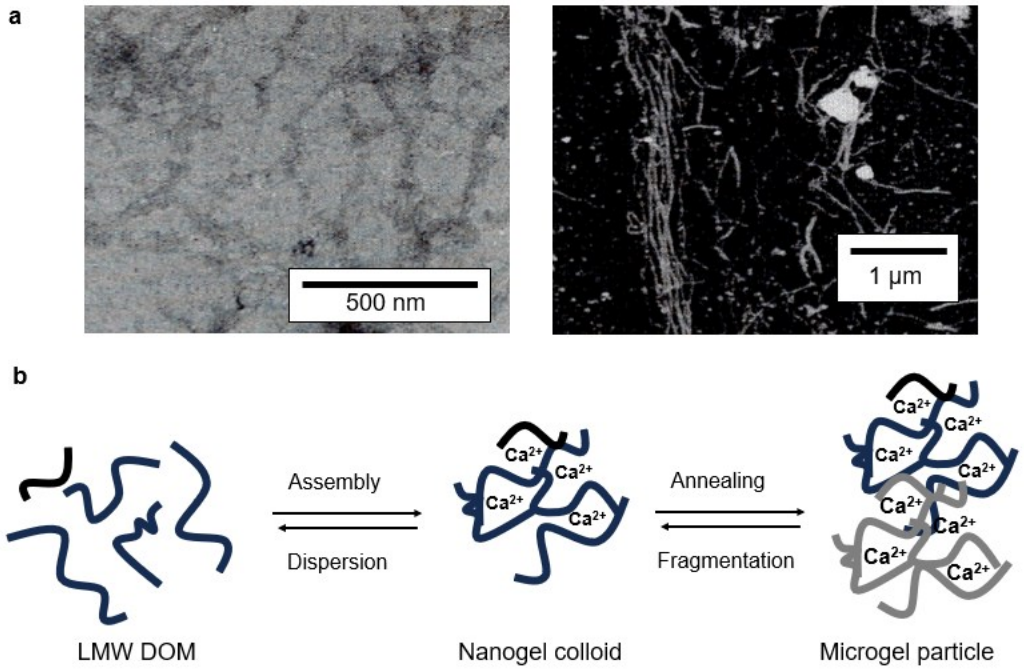

Figure 15: (a) Examples of fractal gel aggregates (left; transmission electron microscopy image of organic colloids from the middle Atlantic Bight surface waters) and entwined fibrils (right; atomic force microscopy image of organic colloids from the surface waters of the Gulf of Mexico) from Santschi et al 1998). (b) Schematic of DOM reversible assembly into nanogels stabilized by entanglement and Ca-bridging, followed by reversible annealing of nanogels into microgels, based on Chin et al. 1998.

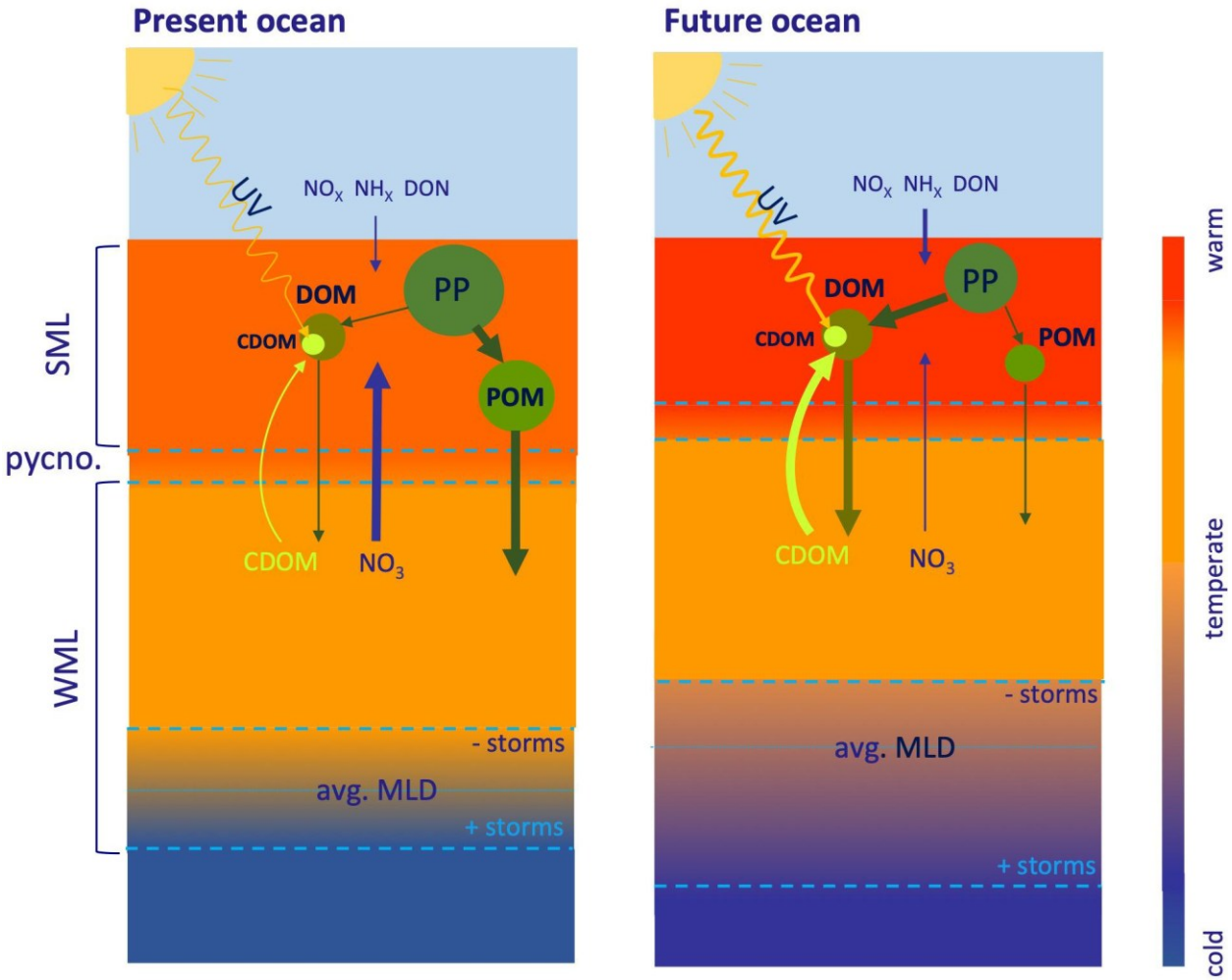

Figure 16: Summary of proposed changes in organic matter reservoirs and transformations in future open oceans. Increased stratification by ocean warming of the surface mixed layer (SML) and stronger pycnocline will decrease the delivery of new nutrients (NO_3 here). Primary production (PP) is predicted to decline with enhanced stratification. Increased temperatures have been shown to increase the release of DOM from PP, though the long-term maintenance of this increase is unknown. Photo-oxidation of DOM is expected to play an enhanced role in a stronger stratified ocean. Particulate organic matter (POM) removal from the surface could be limited in future oceans, though much remains to be determined about these processes. Finally, the average mix layer depth (MLD) in the winter (WML) could decrease with surface warming or increase with presence of enhanced storm events. From Lønborg et al. 2020.

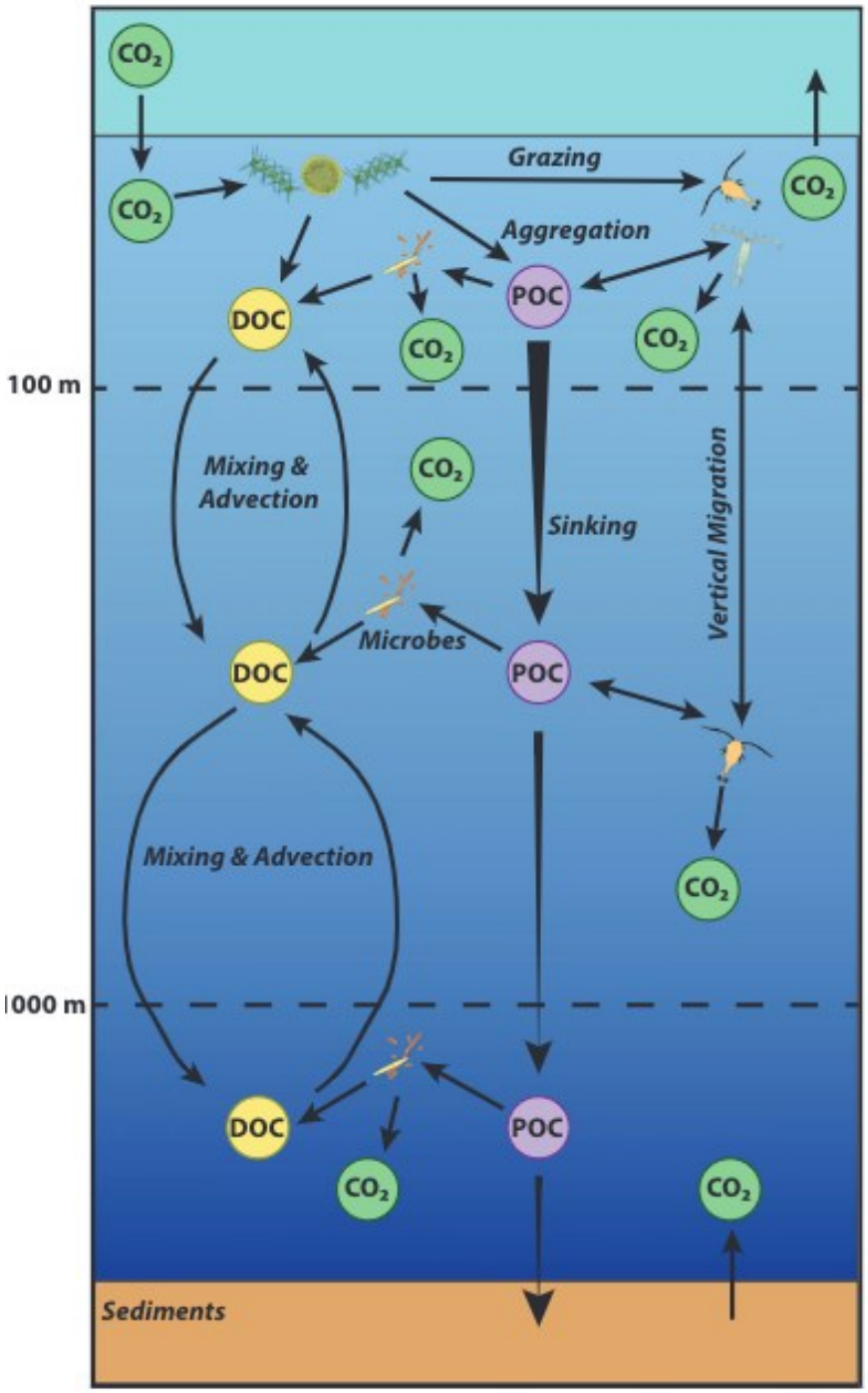

Figure 17: A summary of processes involved in modeling organic matter reservoirs. From Burd et al. 2016.

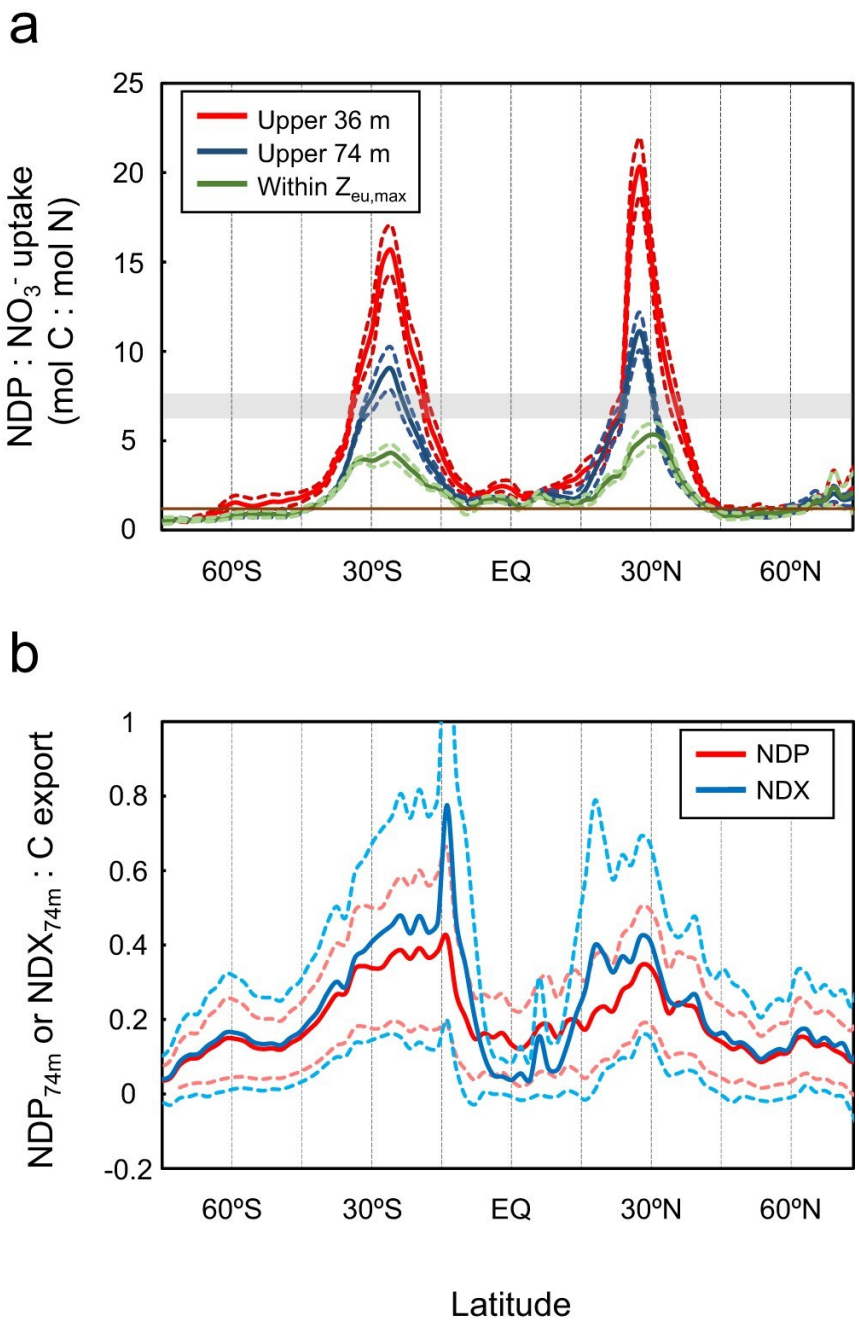

Figure 18: Spatial stoichiometric variability of dissolved organic matter (DOM) as predicted by an artificial neural network. Net DOC production (NDP) relative to nitrate uptake (NO_3^- uptake) C:N increases to significantly higher values above the Redfield ratio (grey line) of 6.625 in low latitudes of subtropical gyres (a). The resulting contribution of NDP (red) or net DOC export (blue) to total C export predicted by satellite suggests that this increase in C:N results in an increased contribution of DOC to total carbon export, as much as >60% in the ultra-oligotrophic South Pacific Ocean (b). From Roshan and DeVries 2017.

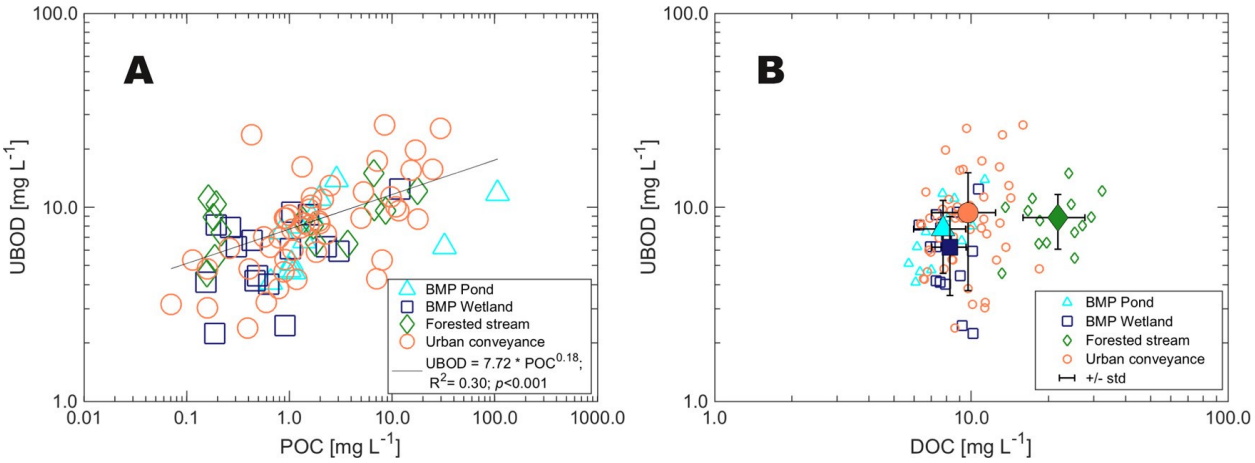

Figure 19: The relationship between biochemical oxygen demand (BOD) versus the concentrations of (A) POC and (B) DOC measured across different water runoff sites after storm events. BOD is an important regulatory metric used to establish effective limits on coastal discharge. Here, ultimate BOD (UBOD) was measured over a longer 28-day incubation period. Shape and colors of points reflect catchment type: best management practices (BMP) wetlands, BMP ponds, forested streams, and urban ditches. BMP retention ponds and constructed wetlands are meant to trap organic matter during peak water discharge, whereas urban sites covered in impervious surfaces provide minimal treatment, and forested streams reflect undeveloped regions. In panel (B) the average DOC and UBOD concentrations for each site type is depicted by a larger filled symbols and error bars that represent the standard deviation. From McCabe et al. 2021.